Available online at www.sciencedirect.com

jmr&t Journal of Materials Research and Technology

journal homepage: www.elsevier.com/locate/jmrt

Original Article

Sulfated and carboxylated nanocellulose for Co^{+2} adsorption

Lucas Tonette Teixeira [a,1], *Wanderson Ferreira Braz* [a,1], *Rogério Navarro Correia de Siqueira* [a,*], *Omar Ginoble Pandoli* [b], *Mauro Cesar Geraldes* [c]

[a] *Departamento de Engenharia Química e Materiais, PUC-Rio, Rio de Janeiro, RJ, Brazil*
[b] *Departamento de Química, PUC-Rio, Rio de Janeiro, RJ, Brazil*
[c] *Departamento de Mineralogia e Petrologia ígnea, UERJ, Rio de Janeiro, RJ, Brazil*

ARTICLE INFO

Article history:
Received 21 March 2021
Accepted 26 July 2021
Available online 4 August 2021

Keywords:
S-CNC
CNF
TEMPO
Acid hydrolysis
Cobalt
Adsorption

ABSTRACT

Regarding metals adsorption from aqueous solutions, nanocellulose emerges as a potential material, due to the many functionalization possibilities and enhanced surface contact area (nanostructured nature). In the present work, sulfated and carboxylated nanocellulose samples were obtained through sulfuric acid hydrolysis (S-CNC) and oxidation by TEMPO (CNF). The obtained nanofibers were characterized through multiple techniques, which XRD data indicated the presence of α-cellulose crystals, with crystallinity indexes equal to 72.3% (S-CNC) and 69.3% (CNF). Expressive morphological differences were revealed, whiskers particles for S-CNC, and elongated nanofibrils for CNF, with average thickness of 9.99 and 5.61 nm, respectively. The desired functionalization with carboxylate groups was evidenced based on FTIR data (CNF). A significant and homogeneous presence of sulfur was evidenced through SEM/EDS (S-CNC). The synthesized nanofibers were next applied to cobalt (Co^{+2}) adsorption from aqueous solutions at room temperature. On both cases, expressive maximum cobalt recoveries have been achieved, 90% (CNF) and 87% (S-CNC), for contact times higher than 30 and 45 min, respectively. The adsorptive capacities evaluated through ICP-OES from liquid phase data (87 mg g^{-1} S-CNC; 90 mg g^{-1} CNF) were both significantly higher than the values determined through LA-ICP-MS (10.5 mg Co g^{-1} S-CNC; 31.5 mg Co g^{-1} CNF).

1. Introduction

Adsorption can be viewed as a possible viable solution for heavy metals removal from water bodies. In this context, biomass derived materials or biomass itself have been both investigated as adsorbent media, with high applicability potential for metals of technological interest. In this context, most of the research conducted and published until the present date is related to the direct use of biomass raw materials,

* Corresponding author.
E-mail address: rnavarro@puc-rio.br (R.N. Correia de Siqueira).
[1] These authors equally contributed to this article.

https://doi.org/10.1016/j.jmrt.2021.07.123

with or without some sort of previous activation chemical treatment. In the work of Zhang et al. [1], activated carbon produced with biomass from the hull of *Xanthoceras Sorbifolia* was employed for adsorption of Co^{+2} from aqueous solutions of 800 mg L^{-1} initial concentration, achieving an equilibrium adsorptive capacity of 126 mg g^{-1} at pH around 5.8, at 50 °C, and 0.8 g of biomass.

The activation of biomass was performed through reaction with an aqueous solution of H_3PO_4, followed by washing, and a final calcination step at 500 °C for 1 h. According to the same authors, equilibrium should have been achieved after 60 min of contact time. Also, the reduction of temperature from 50 °C to 25 °C resulted in an appreciable reduction of the adsorbent capacity to almost 65 mg g^{-1}.

Adsorption of cobalt from aqueous solutions was also investigated by Parab et al. [2], which employed Coir Pith as biomass adsorbent, without any pre-treatment. At 23 °C, for 2 g L^{-1} of adsorbent and Co^{+2} initial concentration of 20 mg L^{-1}, the authors verified that pH has a huge effect on the equilibrium adsorptive capacity for a contact time of 2 h, which increased from 4 mg g^{-1} (pH = 2) to almost 12 mg g^{-1} (pH around 6). They also reported a significant effect of the initial cobalt concentration over the measured adsorptive equilibrium capacity, which, for all experiments was reached after 1 h at pH of 6.0. According to reported data, the maximum equilibrium capacity increased from 8.5 mg g^{-1} for Co^{+2} concentration of 20 mg L^{-1} to 12.4 mg g^{-1} at 50 mg L^{-1}. It is interesting to note that the data of Parab et al. [2] suggest that although the adsorptive capacity increases, cobalt recuperation decreased from 85,4% at 20 mg L^{-1} to 49.6% at 50 mg L^{-1}.

Other sort of biomass already employed for cobalt adsorption from aqueous solutions can be obtained from microalgae cells. In the work from Peres et al. [3], the adsorptive power from *Spirulina* sp. cells at 45 °C is compared with the one observed for commercial charcoal samples, and the effect of the presence of Co^{+2} adhered to the biomass after reaching equilibrium investigated through infrared spectra analysis (FTIR). The adsorptive action of both adsorbents tested has shown to achieve a maximum value for a pH of 6.0 and has proven to be much higher in the case of *Spirulina* sp. in comparison to commercial charcoal. For an adsorbent concentration of 1 g L^{-1} and an initial Co^{+2} concentration of 100 mg L^{-1}, equilibrium was reached for the charcoal fibers only after 400 min, and in the case of the microalgae after a contact time of 100 min. Moreover, the equilibrium capacity for *Spirulina* sp. (25 mg g^{-1}) was a little higher than the one observed for the charcoal sample (20 mg g^{-1}). The authors investigated the effect of the initial Co^{+2} concentration, and, on both cases, although with a much higher effect for the *Spirulina* sp. sample, the equilibrium capacity has been enhanced. When Co^{+2} concentration was equal to 150 mg L^{-1}, the equilibrium capacities of charcoal and *Spirulina* sp. were respectively equal to 34 and 73 mg g^{-1}. According to FTIR analysis, interaction of Co^{+2} with the charcoal particles should develop physically, thereby stimulating a variation in the C–O–C band intensity. In the case of Spirulina, however, a chemical interaction is proposed, through appearance of two new vibration bands at 550 and 800 cm^{-1}, but the authors did not discussed which sort of chemical bonding should be responsible for these bands. Indeed, the much higher effect of Co^{+2} concentration over the adsorption equilibrium in the case of the *Spirulina* sp. sample could be explained by a much stronger bonding (chemisorption) of the cationic species over the biomass particles surface.

As an alternative strategy for metals removing from water solutions, biomass derivative adsorbents can also be interesting candidates. In this context, nanocellulose is one of the most prominent material of biological basis, which can be easily produced from many ligno-cellulosic biomass raw materials [4], and has indeed some properties, which motivates metals adsorption studies, such as, an expressive surface area, directly correlated to dimensions (ex. thickness) far into the nano scale, and also, a high potential towards functionalization, or, in other words, introduction of specific organic functional groups, with the ability to enhance and optimize the adsorptive power of the nanofibers [5]. However, despite of the adsorbent potential yet evidenced, data for Co^{+2} adsorption are very scarce in current literature.

In the case of CNF, nanofibers oxidized under the presence of TEMPO (2,2,6,6-tetramethyl-piperidinyl-N-oxyl) catalyst, earlier studies point out to a significant metal removal potential, with promising kinetics. In the work of Madivoli et al. [6], for example, CNF samples functionalized with citric acid were applied in order to remove Pb^{2+}, Cd^{+2}, Cu^{+2} and Zn^{+2} from aqueous solutions of initial metal concentration equal to 50 mg L^{-1}, at 30 °C and pH equal to 6.0, resulting in significant metal recovery values for Pb^{2+} (80%), Cd^{2+} (80%), Cu^{2+} (76%), and Zn^{+2} (43%), with respective equilibrium adsorptive capacities of 21.7 mg g^{-1}, 23.5 mg g^{-1}, 21.8 mg g^{-1}, and 11.3 mg g^{-1}. Considering the low adsorbent dosage employed (0.1 g) and favored kinetics, evidenced by equilibrium achievement after only 10 min for all cations studied, the proposed citrate functionalization can be evaluated as promising, although the authors did not bring any data for CNF prior to chemical reaction with citric acid.

Sehaqui et al. [7] also studied the application of CNF nanofibers in the adsorption of metal cations from aqueous media, thereby comparing the adsorptive power of both oxidized and non-oxidized nanofibers. The non-oxidized nanofibers were of commercial nature, and main difference from the oxidized sample defined by the substitution of –OH (C^6) groups by –COOH (C^6) units, after interaction with TEMPO under the presence of NaOCl and NaBr. Through NaOCl dosage control, the oxidation degree was varied, and four levels achieved. For the adsorption tests conducted, aqueous solutions containing different metal cations (Cu^{+2}, Zn^{+2}, Ni^{+2}, Cr^{+3}) have been explored, with a prior pH adjustment, nanocellulose dose equal to 1.25 g/L, and initial cation concentration equal to 3.7 mM, at ambient temperature (approx. 25 °C). For all adsorption experiments the contact time was fixed at 20 h. Results pointed out that both pH as well as oxidation degree enhanced the nanofibers adsorptive capacity, and the authors explain it though the concentration of carboxylate units (-COO^-), which work as chemical traps for the cationic species present in solution. Considering Cu^{+2} adsorption, a maximum capacity 135 mg g^{-1} was observed at pH equal to 6.2 and maximum oxidation degree (1.93 mmol COOH), in comparison with 12.2 mg g^{-1} for the non-oxidized sample exposed to the same conditions. Significant metal adsorptive

capacities were also evidenced for the other cationic species studied, and values 58, 49 and 66 mg g^{-1} have been found for Cr^{+3}, Ni^{+2} and Zn^{+2}, respectively, the first two at pH equal to 6.0 and the last at a pH of 5.0, with 20 h of contact time, and 0.1 g of the oxidized nanocellulose of highest oxidation degree.

Data reported by the same authors for Cr^{+3} (14 mg g^{-1}) and Zn^{+2} (2.6 mg g^{-1}), with the un-oxidized nanofibers as adsorbent, suggest a behavior like Cu^{+2}, whereas the oxidation of –OH groups towards –COOH, and its subsequent ionization to $-COO^{-}$, can appreciably enhance the adsorptive power of the nanofibers. On what touches the metal recoveries considering the oxidized sample with a carboxylic content of 1.93 mmol g^{-1}, for Cu^{+2} a value equal to 71.8% was found, and regarding Zn^{+2}, Ni^{+2}, and Cr^{+3}, values respectively equal to 34.1%, 28.2% and 27.6%.

Besides CNF, some works in literature covers the direct use of S-CNC nanofibers for heavy metal adsorption from aqueous solutions. Singh et al. [8], for example, prepared S-CNC samples via acid hydrolysis, followed by functionalization with succinic acid and also through subsequent reaction with ethylenediamine. The authors investigated the adsorption of Cr^{+3} from $CrCl_3$ solution and Cr^{+6} from $K_2Cr_2O_7$ aqueous solutions at room temperature, contact time of 40 min, initial concentration of 25 mg L^{-1}, and adsorbent dose of 2 g. For Cr^{+3}, pH was fixed at 6.5, and cationic recovery varied appreciably among the three samples tested, micrometric cellulose (MC), employed as raw material for CNC synthesis, S-CNC and CNC functionalized by succinic acid, with metal recoveries respectively equal to 42 ± 0.03%, 62.4 ± 0.03% and 94.84 ± 0.06. In the case of Cr^{+6}, recoveries obtained for MC and S-CNC at a pH equal to 2.5 were compared with the one obtained after amination (NNC), considering, besides the pH, the same experimental conditions employed during study of Cr^{+3} adsorption. For MC and S-CNC samples, metal recoveries of 5.36 ± 0.01% and 5.72 ± 0.09% have been obtained, and for NNC, 98.88 ± 0.08%. These results point out that the chemical nature of the molecular groups introduced during functionalization can have a huge effect over the adsorbent potential of the nanofibers.

In the work of Yu at al. [9], S-CNC has been previously synthesized through acid hydrolysis with H_2SO_4, and the obtained nanofibers next functionalized with succinic anhydride (SA-CNC), which were finally applied for Cd^{+2} (pH = 6.0; initial cation concentration of 0.2 g L^{-1}) and Pb^{+2} (pH = 5.5; initial cation concentration of 0.3 g L^{-1}) adsorption studies from 150 mL aqueous solutions at 25 ± 2 °C, with adsorbent dose of 1 g L^{-1}.

It has been observed that equilibrium adsorptive capacity was considerably enhanced through functionalization, and also that, for both metals, equilibrium was reached much faster for S-CNC (t > 6 min) than for SA-CNC (Pb^{+2}:t > 120 min; Cd^{+2}:t > 150 min), probably explained by some sort of steric effect, not mentioned by the authors in the discussion. Considering the adsorptive capacity of Cd^{+2}, the values for S-CNC and SA-CNC have shown to be respectively equal to 8 and 150 mg g^{-1}, and in the case of Pb^{+2}, 48 and 300 mg g^{-1}. Again, it is seen that functionalization can have a strong effect over adsorption kinetics, as well as for the maximum metal capacity achieved in equilibrium. Equilibrium metal recoveries have also proven to be significant for both cations, being respectively equal to 100% in the case of Pb^{+2} and 75% for Cd^{+2}.

Regarding the application of either CNF or S-CNC for Co^{+2} adsorption from aqueous solutions, the few works found do not involve the direct nanofiber use, but application of some composite of either nanocellulose matrix (S-CNC or CNF). In the work of Anirudhan et al. [10], for example, S-CNC samples were functionalized with itaconic acid, and magnetite crystals than allowed to grow on the fiber/solution interface. The nanocomposite was next applied for studying Co^{2+} adsorption from $Co(NO_3)_2$ aqueous solutions, concentration between 50 and 500 mg L^{-1}, temperature fixed at 30 °C, adsorbent dose of 2 g L^{-1}, and pH equal to 6.5. Then cobalt concentration in the liquid phase was monitored as a function of time, and, for initial concentrations varying between 50 and 200 mg L^{-1}, it was evidenced that an equilibrium state was reached after 52 min. Regarding the data obtained at 100 and 150 mg L^{-1}, equilibrium capacities with values respectively equal to 49 and 75 mg g^{-1} have been reached, with corresponding recoveries equal to 98 and 99%. The adsorptive power of the nanocomposite employed is impressive and should be directly associated with the presence of Fe_3O_4 particles, which once negative charged, could contribute for adsorption with extra binding sites for the Co^{+2} cations dispersed in solution.

On what touches nanocomposites of CNF matrix, some interesting results have been reported for hydroxyapatite (Hap) particles precipitated from liquid phase over the surface of CNF nanofibers (Hap–CNF nanocomposite) [11]. The resulting adsorptive power was enhanced, as phosphate groups from Hap act concomitantly with the hydroxyl units, naturally present in the commercial nanocellulose sample used as raw material (NC; thickness between 10 and 70 nm) and carboxylic groups characteristic of CNF, contributing for the final electrostatic interaction with the cationic entities present in solution.

The adsorption batch experiments were performed with initial Co^{+2} concentration of 100 mg L^{-1}, and the effect of adsorbent dose, pH and contact time then investigated. According to the data, the adsorptive power achieves a maximum for an adsorbent dose of 0.5 g L^{-1} and pH equal to 6.0. For all samples (CN, CNF and Hap-CNF), equilibrium was achieved after 400 min, with adsorptive capacities respectively equal to 17.3 mg g^{-1} (CN), 19.8 mg g^{-1} (CNF) and 22.4 mg g^{-1} (Hap-CNF), and cobalt recoveries of 81.5%, 83.8% and 87%.

As pointed out before, there is a visible lack of information in literature regarding the potential use of CNF or S-CNC nanofibers for cobalt (Co^{+2}) adsorption from aqueous solutions, which should be affected by the chemical process employed for producing the nanofibers. In the present work, two well established synthesis routes for nanocellulose production were employed, and the resultant nanofibers tested as

potential adsorbents for cobalt in aqueous solutions. It should be noted that, differently from most works associated with adsorption studies, the adsorptive capacity is quantified through spectrometric techniques both applied to the liquid (remaining cobalt), as well as for the solid (nanocellulose with adsorbed metal) phases.

2. Methods

2.1. Synthesis of S-CNC and CNF

For both S-CNC and CNF nanofibers synthesis, a chemical processing route was applied, using α-cellulose (Sigma Aldrich) as raw-material. In the case of S-CNC, the nanofibers were obtained by sulfuric acid hydrolysis with a 40% (v v^{-1}) sulfuric acid (H_2SO_4) solution. During synthesis, 20 mL of the acid solution was heated up to 60 °C, then 1 g of α-cellulose was added under constant stirring. After 30 min, 50 mL of cold deionized water (4 °C) was added to interrupt the hydrolysis process. Finally, the solution volume was completed up to 200 mL with deionized water, and reaction media removed through centrifugation at 5800 rpm for 15 min (CIENTEC CT-6000). The solid phase was then washed with 50 mL deionized water and next centrifuged under the same conditions. The washing/centrifuging process was performed four times for each sample. In order to possibly reduce agglomeration, the final sulfated nanocellulose suspension was mechanically treated in ultrasound bath (ULTRONIC Q1.8/40A) for 10 min and finally stored under refrigeration.

For the CNF synthesis, 100 mL of deionized water with 1 g of α-cellulose, 0.1 g of NaBr and 0.016 g of TEMPO catalyst were mixed under continuous stirring. The cellulose oxidation reaction begins when 0.3 g (2.5 mL) of 12% NaClO was added, and pH corrected to 10 with 0.1 M HCl solution addition. In order to maintain the pH constant, drops of 0.5 M NaOH solution were added gradually, the solution pH then continuously monitored through an ION PHS-3E pH meter. After 180 min, the pH variation was close to 10,00 ± 0.01, reaching the precision range of the equipment used, so it was considered that the carboxylic substitution had reached its final state. After this period, in order to remove the reaction medium, the suspension was centrifuged at 5800 rpm for 15 min (CIENTEC CT-6000) and the solid phase washed with 50 mL deionized and centrifugated under the same conditions four times. As in the case o S-CNC, in order to reduce agglomeration, the nanocellulose suspension was treated mechanically in an ultrasound (ULTRONIC Q1.8/40A) bath for 10 min, and finally stored under refrigeration.

2.2. Adsorption tests

For the cobalt adsorption tests, the pH of both nanocellulose suspensions (S-CNC and CNF) was previously adjusted to 6.0. In a 250 mL Erlenmeyer flask 1 g of nanocellulose was mixed with 100 mL of 1 g L^{-1} cobalt nitrate solution.

The solution was continuously stirred at 150 rpm in a CIENTEC CT-712RNT benchtop shaker at room temperature. After each desired adsorption time (30–180 min), the liquid phase was separated through centrifugation at 5800 rpm for 15 min (CIENTEC CT-6000R) and analyzed for Co^{+2} concentration through ICP-OES (PERKIN ELMER 7300 DV). The obtained solid phase was washed/centrifuged four times under similar conditions as performed with the nanofibers just after each chemical processing, and next stored in vacuum desiccator for further characterization through SEM-EDS and laser ablation with coupled ICP-MS. The metal recovery was calculated using the Eq. (1):

$$R\ (\%) = [1 - (C_t/C_i)] * 100\% \quad (1)$$

where C_t represents the Co^{+2} concentration for each specified time and C_i its initial concentration, both given in g L^{-1}.

2.3. Atomic force microscopy (AFM)

A 20 μL aliquot of each nanocellulose suspension (S-CNC and CNF) was deposited over a silicon substrate by drop coating and stored in a desiccator for 3 h in order to achieve full water removal and analyzed via AFM (Bruker multi mode 8) with ScanAsyst tip in tapping mode, and scan size equal to 400 nm^2 (CNF) and 2 μm^2 (S-CNC). Nanofiber dimensions were evaluated using Gwyddion software, version 2.55.

2.4. Scanning electron microscopy with energy dispersive spectroscopy (SEM-EDS)

The surface morphology of vacuum dried S-CNC and CNF samples, both before and after cobalt adsorption, were analyzed through SEM (TM3000 HITACHI). The microscope was equipped with a solid-state EDS detector (SWIFT ED3000), whose signal was processed and analyzed with SWIFT ED 1.7.3.0 software, in order to qualitative evaluate the elemental composition over the nanofibers surface, and to construct EDS elemental maps.

2.5. Fourier transform infrared spectroscopy (FTIR)

Vacuum dried 2 mg samples of both nanofibers produced (S-CNC and CNF) were analyzed using a PERKIN ELMER Frontier FTIR spectrometer. Each sample was mixed with 0.198 g of KBr and pressed into small pellets. Next, the transmittance spectra of the fibers were obtained and the main peaks observed were correlated with the appropriate functional groups present in the cellulose molecule.

2.6. Zeta potential

The surface electric potential of each nanofiber once in contact with water at a fixed pH was measured through zeta potential analysis (Zetasizer Nano-ZS from Marvel). Previously to each measurement, each nanocellulose suspension was diluted with deionized water to 200 ppm concentration, and pH was adjusted to 10 with NaOH 0.5M. Measurements were then performed in a pH range between 3.0 and 10.

2.7. X-ray diffraction (XRD)

X-ray diffraction patterns of both S-CNC and CNF nanofibers were obtained with a X'Pert PRO diffractometer (PHILIPS, PANALYTICAL). The analysis was performed in the range

between 13° and 47°, with angular step of 0.02°, and 7 s acquisition time. Next, Rietveld analysis with fundamental parameters was performed for each obtained signal with software TOPAS (Bruker AXS), version 5.0, in order to optimize the unit cell parameters, and also to evaluate the mean crystallite size of the samples. Additionally, the crystallinity degree (C_D) was calculated for each sample using the Eq. (2) [12,13].

$$CD = (I_{22.5} - I_{18})/(I_{22.5}) \quad (2)$$

where $I_{22.5}$ and I_{18} refer to the XRD intensities measured for Bragg angles respectively equal to 22.5° and 18.0° [14].

2.8. Laser ablation with inductively coupled plasma mass spectrometry (LA-ICP-MS)

Since SEM-EDS data for solid phase elemental characterization are only of qualitative level, LA-ICP-MS analysis was used to corroborate the SEM-EDS maps obtained after exposition of the nanofibers to the cobalt containing solution after 180 min exposition time.

Moreover, it is interesting to note, that most works in literature, which are devoted to quantitative evaluate metals adsorption from biomass samples are exclusively based on the chemical analysis (ICP-OES or ICP-MS) of the liquid phase, and not on the metal concentration over the solid fibers or nanofibers. In the present work, however, adsorption is quantitative evaluated from the liquid (ICP-OES) as well the solid phase point of view, which is based on the quantification (mg g^{-1}) of the cobalt amount adhered to the fibers surface, or in other words, to quantitative evaluate the adsorptive capacity achieved after 180 min. Therefore, each dry, pressed sample undergoes a laser ablation (Excimer 193, PhotonMachine) with energy of 2.78 J cm^{-2}, at a frequency of 3 Hz, for 10 s, with continuous firing and a beam diameter of 10 μm, resulting in 10 shots for each sample. The volatized material is then dragged into a He current flow, thus transporting the molecular fragments for chemical analysis in an ICP-MS (NEPTUNE Plus Multicollector, ThermoScientific). Previously to each measurement, a calibration curve was constructed with the following standards: NIST 610 and NIST 612.

3. Results

3.1. AFM and SEM-EDS analysis

The characteristic morphology of both nanocellulose samples can be appreciated in Fig. 1, and the corresponding SEM images (Figs. 2a and 3a). Also, elemental composition evaluated trough EDS maps is reported in Figs. 2b–d and 3b–d. As carbon was contained in the sample holder, its presence was not considered for evaluating EDS signal.

3.2. FTIR analysis

The FTIR spectra of both nanocellulose samples (CNF and S-CNC) are presented in Fig. 4.

3.3. XRD analysis

The Rietveld analysis results for S-CNC and CNF samples are presented in Fig. 5a and b, and the optimized lattice parameters and mean crystallite sizes on Table 1. The Crystallinity Degree calculated by Eq. (2) to CNF and S-CNC were 69.3 ± 0.7 and 72.3 ± 0.7, respectively. Crystallites average size calculated by Rietveld analysis were 4.7 and 4.6 nm, to CNF and S-CNC, respectively.

3.4. Zeta potential

Prior to the adsorption tests, the effect of the nanofibers suspensions pH over the measured zeta potential was investigated (Fig. 6). Such analysis was performed in order to identify a pH range of minimum and negative potential, which could be associated with a maximum negative surface charge, thereby improving coulombic interaction between Co^{+2} and the nanofibers contained in the suspension.

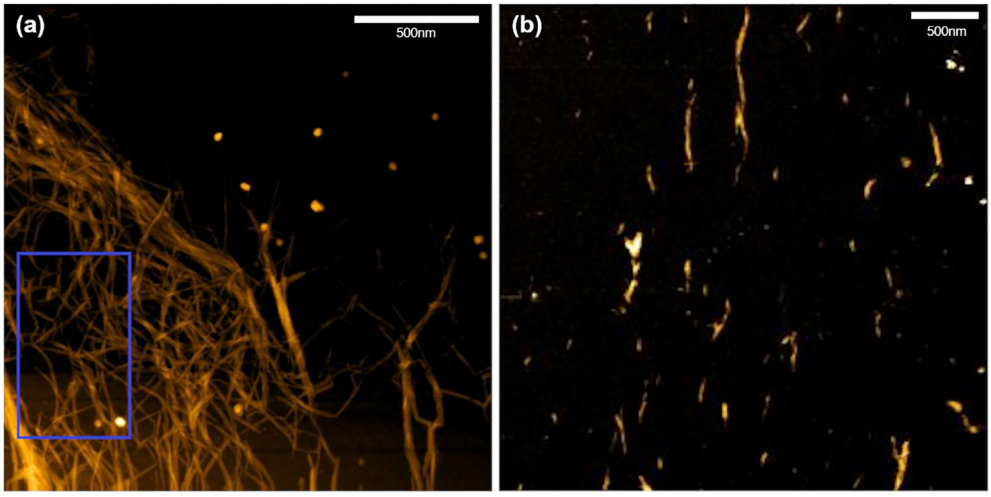

Fig. 1 – AFM images of CNF (a) and S-CNC (b) samples.

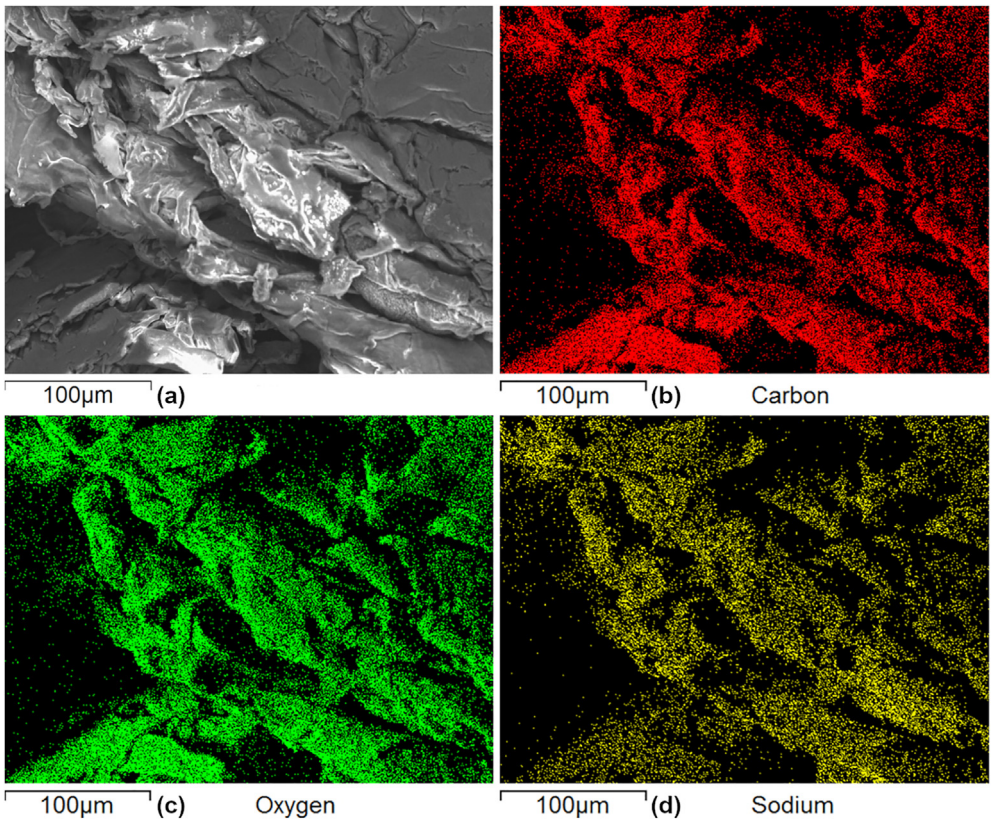

Fig. 2 – SEM image (a), EDS map for C (b), EDS map for O (c) and EDS map for Na (d) of dried CNF sample.

3.5. *Adsorption tests*

In Fig. 7, the pourbaix diagram of the system Co-O-H at 23 °C is presented, and in Fig. 8, data for cobalt recovery as a function of time, calculated by use of Eq. (1) for both nanocellulose samples.

3.6. *SEM/EDS characterization after Co^{+2} adsorption*

The corresponding EDS spectra and EDS map of each dried sample after a 180 min exposition to cobalt solution (CNF–Co and S-CNC–Co) can be appreciated in Figs. 9 and 10.

4. Discussion

4.1. *AFM and SEM analysis*

The AFM data reveal a considerable morphological difference among the nanofibers. In the case of CNF (Fig. 1a) clusters of nanofibrils can be evidenced, with thickness in the nano scale and micrometric length, consistent with earlier literature results [15–18]. Regarding the S-CNC sample (Fig. 1b), particles of much shorter length in comparison to CNF and non-uniform thickness can be observed. Such morphology is in accordance with the literature and may have a close relation to a more aggressive chemical treatment inherent to acid hydrolysis [19–21]. For the CNF sample, the nanofibers thickness was evaluated through digital processing of the depicted area in Fig. 1a, revealing the presence of nanofibers with a thickness equal to 5.61 ± 0.48 nm, close to the mean value of 3.5 nm reported by Isogai [15]. It should be noted that regarding CNF nanofibers length, its micrometric magnitude order lied outside the measurement range characteristic of the microscope employed, and therefore, could not be evaluated.

The present microscopic data suggests that for CNF, the synthesis route employed can lead to nanofibrils with low polydispersity regarding their thickness and with a significant agglomeration tendency. For the S-CNC sample, both average length and thickness, considering all region displayed in Fig. 1b, have been determined and shown to be, respectively, equal to 63.89 ± 41.51 nm and 9.99 ± 2.58 nm. Such a significant length difference should have a strong connection with the nature of the reaction medium used in each case, much more aggressive in the case of acid hydrolysis due to H_2SO_4 presence, and, in the end, contributing to a more effective defibrillation, and shorter nanofiber length. When compared to literature, S-CNC average length is in the range of previous AFM data: 45.9 nm [19], 132 ± 55 nm [22] and 183 ± 88 nm [22].

Also, according to literature, nanocellulose source can affect considerably the nanofibers length and thickness (diameter), which vary respectively between 100 - 300 nm and 3–5 nm for wood pulp, 100–150 nm and 5–10 nm for cotton, and for sisal between 100 - 300 nm and 3–5 nm [23].

The CNF sample analyzed through SEM/EDS, demonstrated the presence of fiber clusters with rough surface and

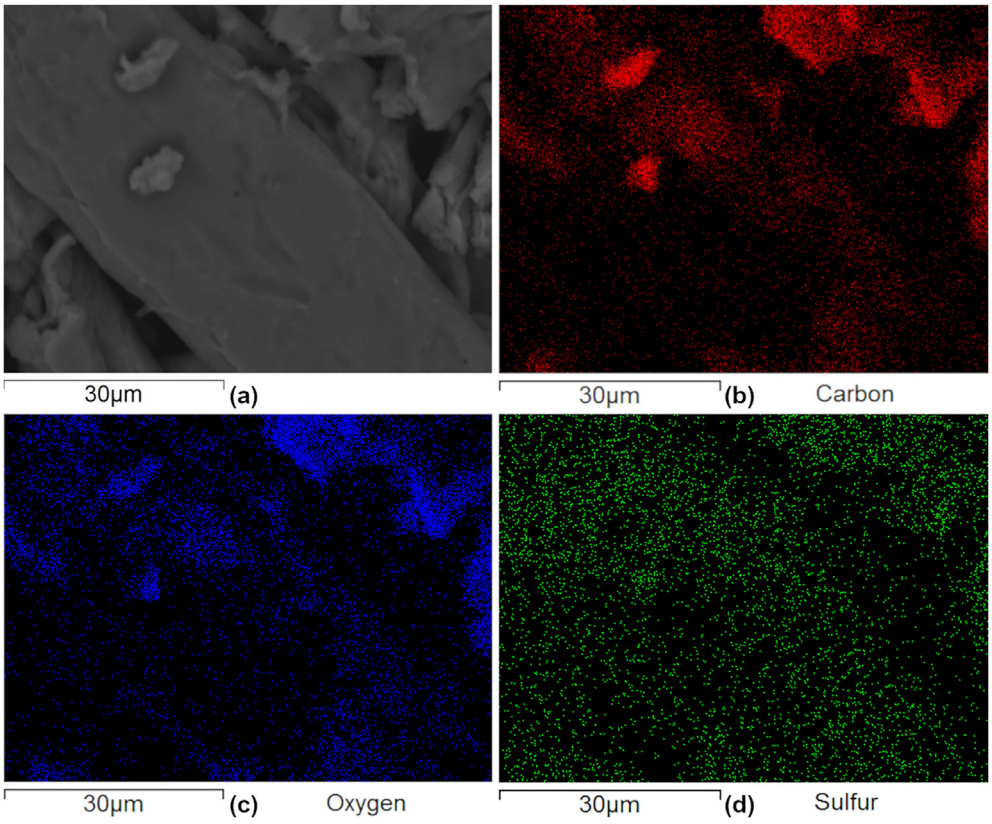

Fig. 3 – SEM image (a), EDS map for C (b), EDS map for O (c) and EDS map for S (d) of dried S-CNC sample.

strong tendency towards charging (Fig. 2a). The EDS spectra (Fig. 2b) indicated a significant presence of C and O, both natural elements present in the original cellulose structure, but also measurable quantities of chlorine and sodium, associated with the reaction media (NaOCl and NaOH). The significant contrast associated with sodium evidenced in the EDS map (Fig. 2c), serves as evidence in favor of the desired introduction of carboxylic groups (COOH), which through chemical interaction with solution can lead to formation of sodium carboxylate units (-COONa).

The SEM/EDS analysis of S-CNC sample also revealed fiber agglomerates, but of more uniform surface, and no charging tendency (Fig. 3a). The corresponding EDS signal revealed, besides C and O from cellulose structure, a measurable amount of sulfur (Fig. 3c), which distributes homogeneously throughout the sample, and serve as indicative of the partial substitution of

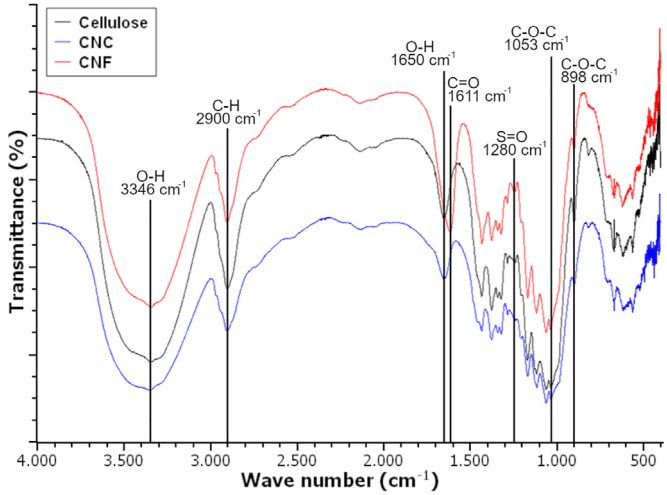

Fig. 4 – FTIR spectra to Cellulose, CNF and S-CNC samples before adsorption tests in order to confirming the functionalization of samples.

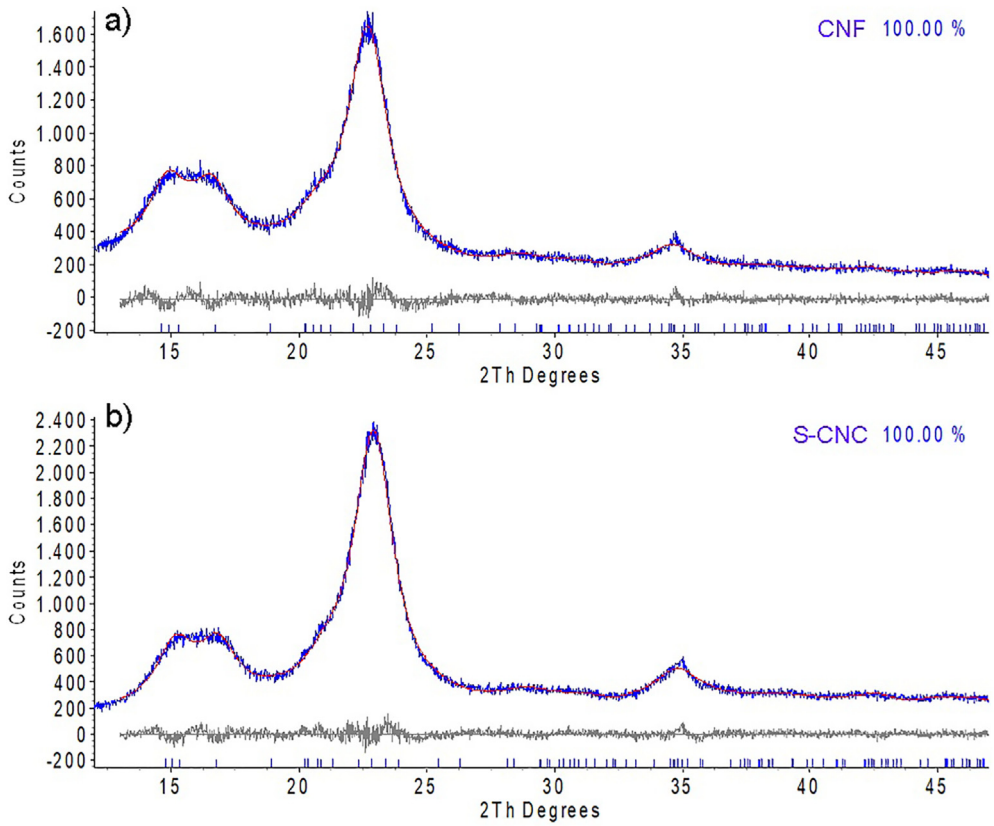

Fig. 5 – Rietveld refinement results for CNF (a) and S-CNC (b) samples.

the original –OH units for the desired $-OSO_3H$ groups. This assumption is reinforced by the fact that, prior to SEM analysis, the solid sample was washed/centrifuged four times. Therefore, it is presumed that most of residual sulfate ion (SO_4^{-2}) from the aqueous media, probably physiosorbed onto the fibers surface, could then be eliminated.

4.2. *FTIR spectra*

Regarding the cellulose spectrum, it is possible to identify bands relative to the presence of hydroxyl groups (-OH), C–H bonds and C–O–C units. The bands at 3200 and 3346 cm^{-1} are associated to stretching vibrations of the O–H bond in hydroxyl groups [6]. The band centered at 2900 cm^{-1} is attributed to asymmetric and symmetric stretching vibrations of aliphatic C–H bonds, and the band located at 1053 cm^{-1} is related to C–O–C pyranose ring vibration [6]. Additionally, for both S-CNC and CNF there is a reduction of intensity for the band at 898 cm^{-1}, which, according to literature, is related to glycosidic bonds β-1,4 (C–O–C) stretching vibrations, resultant from a reduction of cellulose chain length [24]. In the case of the CNF sample, the main difference, when compared to cellulose, is a vibration band at 1611 cm^{-1}. This wavelength is associated to carboxylate COO^- asymmetric stretching vibrations [25], corroborating the substitution of –OH, as suggested by the sodium contrast evidenced through SEM (Figs. 2 and 3). The asymmetric stretching vibration bands of S–O bonds, which are correlated to the presence of inserted organic sulfate group ($R-OSO_3H$), were expected near a wave number of 1280 cm^{-1} [17,26]. Indeed, the FTIR data for the S-CNC sample indicates a signal variation in this region, with the appearance of a "slope", although, considering the present signal intensity, no associated transmittance band could be detected. This could be explained by the superposition with signals related to C–O–C or C–O–H vibrations, whose bands, according to literature, should lie between 1300 and 1000 cm^{-1} abundant groups in the original cellulose macromolecule.

Table 1 – Fitting quality (GOF) and refined lattice parameters after Rietveld analysis for cellulose, CNF, and S-CNC samples.

Material	GOF	Lattice parameters					
		a (Å)	b(Å)	c(Å)	α(°)	β(°)	γ(°)
CNF	1.19	10.36	6.492	5.987	80.53	117.5	114.0
S-CNC	1.18	10.35	6.430	5.979	80.23	117.8	113.8
Cellulose [27]	2.41	10.40	6.717	5.962	80.37	118.1	114.8

4.3. *Rietveld analysis of XRD data*

After Rietveld analysis of data presented in Fig. 5, the sole presence of α-cellulose was observed on both samples. All optimized lattice parameters have shown to be close to literature (Table 1). The low magnitude of the difference between calculated and experimental signals (bottom grey line

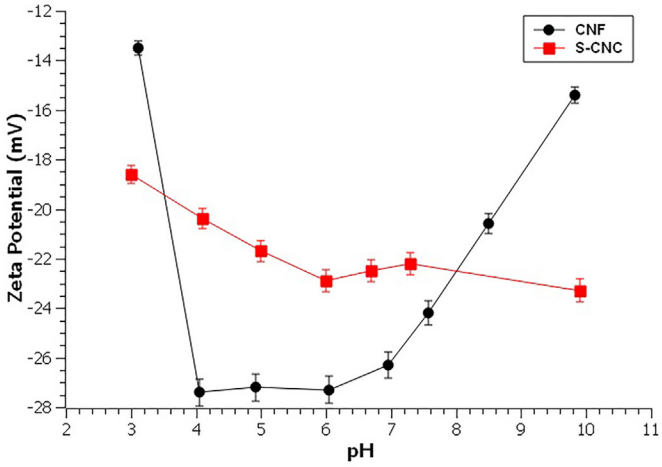

Fig. 6 – Zeta-potential as a function of pH for S-CNC and CNF samples.

in Fig. 5), together with the low GOF values (close to unity), confirm the refinement quality. It is interesting to observe that the mean crystallite sizes of both S-CNC and CNF are quite similar, and lower than 5 nm, indicating that the smallest crystalline units present in the nanofibers should have nanoscale dimensions, and consistent with the low mean thickness determined through AFM discussed earlier. It is important to note some small discrepancies between the lattice parameters determined by Nishiyama et al. [27] and the values obtained in present work, which could be explained by data fitting quality. In the case of the one carried out by Nishiyama et al. [27], a much higher GOF (2.41) was reported, and therefore, should have a lower quality in comparison to the fitting performed in the present work. Additionally, it is observed that both nanocelluloses are associated with similar crystallinity indexes, 72.3% for S-CNC and 69.3% for CNF. These values fit in the expected ranges according to literature, 63.8–83.8% for CNF [28] and from 62 to 75% for S-CNC [29], and the variations can be explained by the cellulose source and or reaction conditions employed.

4.4. *Zeta potential measurements*

The results of electrophoretic mobility measurements of the nanocellulose particles dispersed in solution, presented in Fig. 6, for both S-CNC and CNF, indicate a negative zeta-potential for the whole pH range considered. The negative net-charge of the solid surface, originated through the presence of anionic species (-COO^- or $-OSO_3^-$) is the driving force for the adsorption of Co^{+2} cations present in solution. The observed reduction of the measured zeta potential for pH values higher than 3.0 can then be explained as a dislocation of the ionization equilibrium of –COOH and $-OSO_3H$ units, thereby forming, respectively, –COO– and $-OSO_3$- ionized groups. After full ionization, a constant value of -22.1 ± 1 mV is achieved for S-CNC. Regarding the suspension containing CNF nanofibers, the minimum value at -27 ± 1 mV should indicate the achievement of an equivalent state regarding the ionization of the original carboxylic units. It is important to note, that similar zeta potential values at a pH of 6.5 were reported earlier in literature, –30 mV for CNF [11] and –25 mV for S-CNC [30].

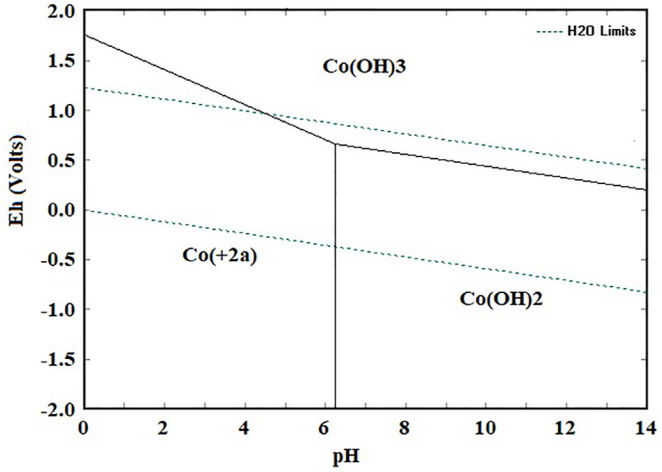

Fig. 7 – Pourbaix diagram for the Co–O – H system at 23 °C.

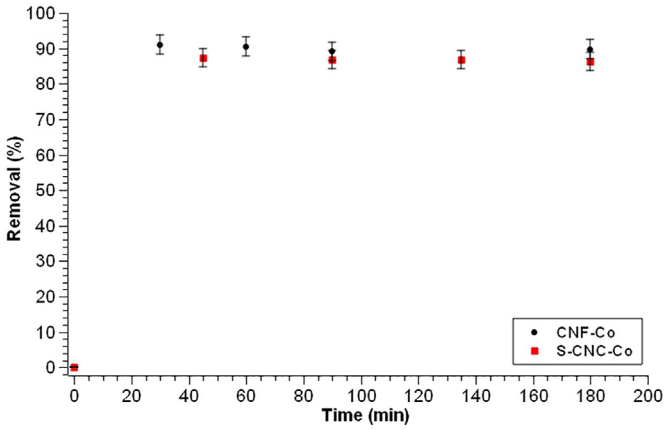

Fig. 8 – Co^{+2} recovery at room temperature as a function of contact time for CNF and S-CNC samples.

Finally, in the case of CNF sample, the measured zeta potential magnitude gets lower as pH becomes higher than 6.0. This could be possibly explained by the partial agglomeration tendency of the nanofibrils, indeed suggested by AFM data presented earlier (Fig. 1a). Through agglomeration, surface area reduces, and also the repulsive interaction among the fibers, thereby leading to a suspension stabilization and lower electric potential. However, such reasoning deserves deeper investigation, for example, through DLS particle size distribution analysis.

4.5. *Cobalt adsorption*

The Pourbaix diagram for the system Co–O – H contained in Fig. 7, which was constructed at 23 °C with HSC software [31], indicates that cobalt should be present as free Co^{+2} species for pH values lower than approximately 6.3. Therefore, as prior to each adsorption test, nanocellulose suspension pH was set at 6.0, cobalt adsorption should be associated with diffusion of Co^{+2} species towards each nanofiber surface, possibly establishing chemical bonds with the available -COO- and $-OSO_3$- groups. It should also be noted that during all adsorption tests, no visual evidence of any precipitate formation ($Co(OH)_2$) was detected, as well as through SEM analysis after 180 min exposition time (Fig. 10).

Based on the analysis of data contained in Fig. 8, it can be observed that a saturation condition is reached on both cases, after 30 min for CNF and 45 min for S-CNC, with similar mean recovery values, 87 ± 2% (S-CNC) and 90 ± 3% (CNF). Therefore, considering an initial concentration of 1 g L^{-1}, and the fact that for each gram of nanocellulose 100 mL Co^{+2} has been employed, adsorptive capacity values respectively equal to 87 and 90 mg g^{-1} were found. Considering the low temperature involved (approx. 23 °C), and the fact that the time interval for equilibrium establishment was lower or equal to 45 min, these results suggest that functionalization through carboxyl or sulfate groups, should contribute significantly for an efficient cobalt adsorption, both from a kinetic as well thermodynamic point of view. It should be noted that it is expected that part of the nanostructured content could not be efficiently separated from the liquid phase for the centrifugation conditions employed in the proposed methodology (5800 rpm, 15 min). Therefore, the authors believe that the actual recovery values measured could be even higher, than the values reported (Fig. 8).

Comparing the adsorptive behavior of the present nanofibers with previously literature results for cobalt [1–3,10,11] and or other metals [6–9], it should be noted that, in the present case, either higher recoveries have been achieved or an enhanced adsorption kinetics is observed. In the work of

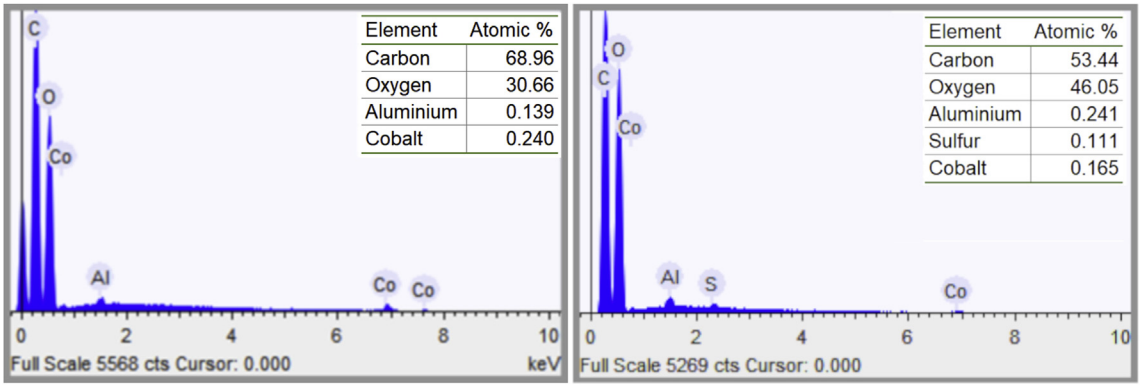

Fig. 9 – EDS spectrum and atomic fractions for CNF–Co (a) and S-CNC–Co (b) dried samples after a contact time of 180 min.

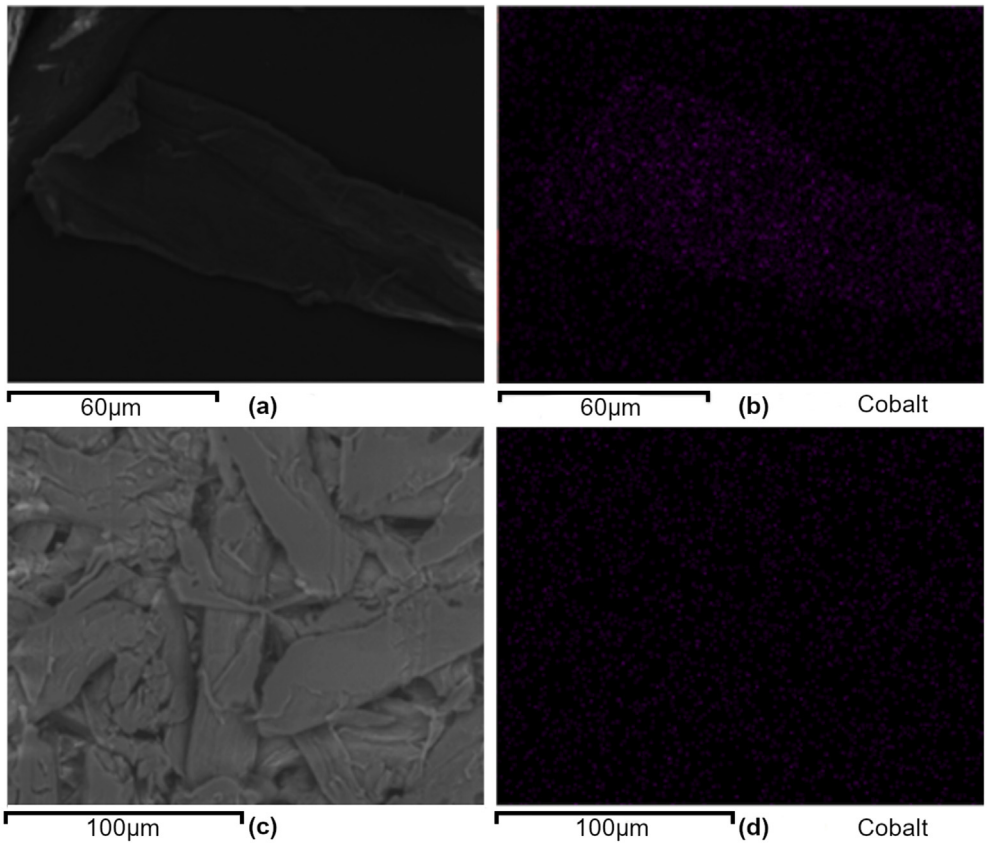

Fig. 10 – EDS maps for CNF–Co (a, b) and S-CNC–Co (c, d) dried samples after a contact time of 180 min.

Zhang et al. [1], for example, equilibrium is reached at 25 °C only after 60 min, and maximum metal recovery was considerably lower (65%), with an initial concentration and adsorbent dose of similar magnitude in comparison with the present investigation. For the experiment conducted at 50 °C, however, a significant higher capacity was reported by the authors (126 mg g^{-1}), but they did not discuss if such an effect should be of either kinetic or thermodynamic nature. Regarding the work of Parab et al. [2], although the evaluated metal recovery (85%) lies very close to the one determined in the present work (87% for S-CNC and 90% for CNF), equilibrium is reached after only 60 min. Considering temperature and initial concentration employed by the authors (25 °C, 0.02 g L^{-1}), it can be concluded that coir-pith fibers induce an adsorption behavior of less favored kinetics in comparison to the CNF or S-CNC nanofibers employed in present investigation.

The same scenario, with a few exceptions, is observed considering the works associated with the direct use of CNF, S-CNC or some functionalization thereof as adsorbent. In the work of Madivioli et al. [6], which functionalized CNF by citrate groups, for example, a much faster achievement of equilibrium was observed (10 min), however, a much lower initial concentration was employed (0.05 g L^{-1}), resulting in a much lower time for adsorption equilibrium establishment, and also, much lower maximum adsorptive capacities (11–21 mg g^{-1}).

On the other hand, the carboxylate units of CNF show an expressive affinity towards interaction with Cu^{+2} cations, as evidenced by the results presented in the work of Sehaqui et al. [7]. Both the cation initial concentration (0.23 g L^{-1}) and adsorbent dose (1.25 g L^{-1}) are both much lower than the values employed in the present work, although a significantly higher capacity was reported (126 mg g^{-1}). However, besides not reporting temperature, kinetic data was also absent. The fixed contact time considered (20 h), is of much higher magnitude than the one necessary for equilibrium establishment according to the present investigation, which should be lower or equal than 30 min for CNF and 45 min for S-CNC.

Considering the fact that both cations are divalent (Cu^{+2} and Co^{+2}) and that the same functionalization is involved (-COOH), the concentration of carboxylic units, which could be higher in the work of Sehaqui et al. [7], and which have not been precisely controlled in the present work, could explain the main differences found.

Functionalization of SNC nanofibers through reaction with itaconic acid, followed by substitution of the carboxylic unit for amine groups has proven to be an interesting way for enhancing the adsorbent power for both +3 or +6 chromium extraction from aqueous solutions, and expressive maximum recoveries values have been reported, 98.8% for Cr^{+6} at pH equal to 2.5, and 94.8% for Cr^{+3} at pH of 6.0 [8], both for a cation initial concentration of 0.25 g L^{-1}, which is considerably lower than the one employed in the present work. These last recovery

values, although of similar magnitude, are both higher than achieved in the present work with either CNF (90%) or S-CNC (87%). It should be noted, however, that in the work of Singh et al. [8], no information is given regarding temperature, as, well as the adsorbent concentration. Moreover, as the contact time was fixed at 40 h, no information was given regarding the adsorption kinetics, which, as said before, can be considered quite satisfactory for both nanofibers studied in the present investigation, and can vary considerably regarding the functionalization type employed. Adsorption kinetics for both nanocellulose fibers investigated in the present work appears to be much more favorable than the one observed for adsorption of Cd^{+2} or Pb^{+2} over CNC nanofibers functionalized with succinic anhydride, as reported by Yu et al. [9].

According to these data, both obtained at a similar pH (6.5) and temperature (25 °C), as employed in the present study, equilibrium should be expected only after 120 min in the case of Pb^{+2}, and 150 min for Cd^{+2}. It should be noted that the initial metal concentration was on both cases much lower than the one employed in the present work (1 g L^{-1}), being equal to 0.3 g L^{-1} in the case of Pb^{+2} and 0.2 g L^{-1} for Cd^{+2}. As these cations are divalent, and similar in size to Co^{+2}, the much higher volume of the anhydride units could be associated with some steric hindrance, thereby making the cation approach more difficult, and in the end contributing for a slower approach to equilibrium state.

Considering Co^{+2} adsorption under the presence of CNF, it is worth noting that, although the mean maximum recovery found in the present work (90%) lies close to the values reported by Narwade et al. [11] at the same pH for CNF (83.8%), and CNF-Hap composite (87%), adsorption kinetics appears to be much more efficient in the present case, as ICP-OES data suggest that equilibrium should be achieved for a time interval less than 30 min, in comparison to 400 min, as reported by Narwade et al. [11]. In this context, it is worth noting that the authors have employed a much lower Co^{+2} initial concentration (0.1 g L^{-1}), than the value employed in the present research (1 g L^{-1}). The much higher saturation time found by Narwade et al. [11] for both CNF and CNF-Hap composite could be explained by the fact that they used a previously prepared CNF sample as raw-material, probably through some mechanical processing route, whose mean "diameter" lied in the range between 10 and 70 nm [11], strongly suggesting a much lower nanostructured content, and consequently contact area, in comparison with the CNF produced in the present work.

Finally, the Co^{+2} adsorptive power evidenced for the S-CNC nanofibers synthetized in the present article can be comparable to the one observed by Anirudhan et al. [10]. Although the present maximum recoveries are both lower than the one determined by the last authors (98%) for the same pH value (pH = 6.0), a higher time (52 min) was necessary for achievement of equilibrium in the work of Anirudhan et al. [10], in comparison to the present research (<45 min), even considering a much lower initial Co^{+2} concentration (0.1 g L^{-1}), and adsorbent dose (2 g L^{-1}), in comparison with the values used in the present study. The authors believe that through a proper optimization of the synthesis conditions the concentration of $-SOO_3^-$ groups could be enhanced, thereby maximizing the final metal recovery achieved. The same could also be said regarding the insertion of carboxylic units during CNF synthesis under the presence of TEMPO.

4.5.1. *SEM analysis after cobalt adsorption*

Through SEM analysis of the solid phase after 180 min exposition to the cobalt aqueous solution, both EDS spectra analysis (Fig. 9) and EDS maps (Fig. 10) suggest, although in a qualitative level, the presence of adsorbed cobalt dispersed over both nanofibers surface, and also indicating a lower concentration for the S-CNC–Co sample. Therefore, in order to have a quantitative appreciation of the actual cobalt concentration adhered to the fibers surface after 180 min, LA-ICP-MS analysis was performed for the same dried samples observed through SEM.

4.5.2. *Adsorptive capacity through LA-ICP-MS*

In order to have a perspective of the adsorptive capacity from the adsorbent point of view, each washed and dried nanofiber sample (CNF or S-CNC), after a 180 min of contact time, was characterized through LA-ICP-MS. The results indeed suggest that for CNF–Co a much higher cobalt concentration should be present, being equal 31.5 mg g^{-1}, in comparison to 10.5 mg g^{-1} found for S-CNC–Co, although much lower values in comparison to the ones obtained from concentration evaluation from the liquid phase, 90 mg g^{-1} for CNF and 87 mg g^{-1} for S-CNC. These results suggest that part of the Co^{+2} cations previously adsorbed on the nanocellulose chains of CNF or S-CNC, could have been removed through repeated washing/centrifugating cycles. It is interesting to note, that such cation leaching out effect was already evidenced in literature through ICP-MS data for Cu^{+2} adsorption in Bamboo fibers [32]. Moreover, the differences between the adsorptive capacities measured for CNF–Co (31.5 mg g^{-1}) and S-CNC–Co (10.5 mg g^{-1}) are consistent with the EDS spectra (Fig. 9) and EDS-map (Fig. 10), which both suggest a more significant concentration of the metal in the case of CNF. The authors believe that the higher adsorptive capacity of CNF could be explained by a higher concentration of –COOH (CNF) in comparison to $-SO_3H$ groups in S-CNC, or evidence of a stronger interaction of cobalt and the available carboxylic units, corroborated by the EDS-map contrasts of Na (-COONa) and S (Figs. 2c and 3c).

5. Conclusions

In the present work, sulfated (S-CNC) and carboxylated (CNF) nanocellulose samples have been successfully synthesized. The samples morphology exhibited significant differences, being similar to whiskers in S-CNC and of nanofibrils of micrometric length in CNF. On both cases, the mean thickness evaluated through AFM, pointed to the presence of a significant nanostructured content, and was equal to 5.61 ± 0.48 nm for CNF and 9.99 ± 2.58 nm in the case of S-CNC.

The XRD data with Rietveld analysis revealed the presence of α-cellulose crystals on both samples, of very similar mean crystallite size (4.6 nm for S-CNC and 4.7 nm for CNF). According to FTIR analysis for the CNF sample, as expected, -COONa groups should have been inserted in the C^6 position, and a resultant vibration band around 1611 cm^{-1} was

accordingly observed. Regarding S-CNC, due to possible superposition of bands of C–O–C and C–O–H bonds, present naturally in the cellulose molecular structure, the sulfate group (-OSO_3) stretch vibrational band (around 1280 cm^{-1}) could not be observed. Indeed, the SEM/EDS analysis conducted on both nanocellulose samples indicated the presence of sodium in the case of CNF and of sulfur in the case of S-CNC, supporting the successful functionalization during synthesis on both cases.

Both nanocellulose types evidenced a strong adsorptive potential towards Co^{+2} removal from aqueous solutions at ambient temperature (approx. 23 °C), with maximum mean recoveries of 90 ± 3% for CNF and 87 ± 2% for S-CNC, and contact times equal or higher than 30 min for CNF and 45 min for S-CNC. The presence of cobalt in the solid phase after 3 h contact time was quantitative confirmed on both cases through laser ablation ICP-MS coupled analysis, resulting in concentrations of 31.5 mg Co g^{-1} (CNF) and 10.5 mg of Co g^{-1} (S-CNC). The lower adsorptive capacities found through solid phase ICP-MS analysis after laser ablation most probably resulted from metal leaching from nanofibers surface motivated through repeated washing/centrifugating steps. The lower cobalt content on S-CNC after cobalt adsorption was also verified through EDS analysis. Additionally, the higher cobalt adsorptive capacity achieved in the case of CNF was confirmed though LA-ICP-MS, and could be possibly explained by its higher sodium carboxylate (-COONa) concentration (higher functionalization degree) in comparison to $-SO_3H$ in S-CNC. This information is corroborated by the constructed SEM/EDS maps obtained for each solid nanocellulose sample just after chemical synthesis.

Regarding the adsorptive potential of S-CNC or CNF, the present results can be classified as quite promising, and should stimulate both a quantitative evaluation and modelling of Co^{+2} adsorption kinetics, as well as a quantification of the functionalization degree achieved on both samples under the proposed reaction conditions.

Declaration of Competing Interest

None declared.

Acknowledgements

The authors specially thank for the Spectroscope Atomic Laboratory (LABSPECTRO) from Chemistry Department of PUC-Rio, and X-ray Crystallography and Diffraction Laboratory from Brazilian Center for Physical Research (CBPF). The authors thank to CAPES and CNPQ for research financial support during the development of the research.

REFERENCES

[1] Zhang X, Hao Y, Wang X, Chen Z. Adsorption of iron(III), cobalt(II), and nickel(II) on activated carbon derived from Xanthoceras Sorbifolia Bunge hull: mechanisms, kinetics and influencing parameters. Water Sci Technol 2017;75(7–8):1849–61. https://doi.org/10.2166/wst.2017.067.

[2] Parab H, Joshi S, Sudersanan M, Shenoy N, Lali A, Sarma U. Removal and recovery of cobalt from aqueous solutions by adsorption using low cost lignocellulosic biomass - coir pith. J Environ Sci Health Part A 2010;45:603–11. https://doi.org/10.1080/10934521003595662.

[3] Peres Enrique C, Cunha Jeanine M, Dortzbacher Gabriel F, Pavan Flávio A, Limac Éder C, Foletto Edson L, et al. Treatment of leachates containing cobalt by adsorption on Spirulina sp. and activated charcoal. J Environ Chem Eng 2018;6:677–85. https://doi.org/10.1016/j.jece.2017.12.060.

[4] Phanthong P, Reubroycharoen P, Ha X, Xu G, Abudula A, Guan G. Nanocellulose: extraction and application. Carbon Resour Convers 2018;1(1):32–43. https://doi.org/10.1016/j.crcon.2018.05.004.

[5] Mahfoudhi N, Boufi S. Nanocellulose as a novel nanostructured adsorbent for environmental remediation: a review. Cellulose 2017;24:1171–97. https://doi.org/10.1007/s10570-017-1194-0.

[6] Madivoli E, Kareru P, Gachanja A, Mugo S, Murigi M, Kairigo P, et al. Adsorption of selected heavy metals on modified nano cellulose. Int Res J Pure Appl Chem 2016;12:1–9. https://doi.org/10.9734/IRJPAC/2016/28548.

[7] Sehaqui H, Larraya UP, Liu P, Pfenninger N, Mathew AP, Zimmerman T, et al. Enhancing adsorption of heavy metal ions onto biobased nanofibers from waste pulp residues for application in wastewater treatment. Cellulose 2014;21:2831–44. https://doi.org/10.1007/s10570-014-0310-7.

[8] Singh K, Arora JK, Sinha TJM, Srivastava S. Functionalization of nanocrystalline cellulose for decontamination of Cr (III) and Cr(VI) from aqueous system: computational modeling approach. Clean Technol Environ Policy 2014;16(6):1179–91. https://doi.org/10.1007/s10098-014-0717-8.

[9] Yu X, Tong S, Ge M, Wu L, Zuo J, Cao C, et al. Adsorption of heavy metal ions from aqueous solution by carboxylated cellulose nanocrystals. J Environ Sci 2013;25(5):933–43. https://doi.org/10.1016/S1001-0742(12)60145-4.

[10] Anirudhan TS, Shainy F, Deepa JR. Effective removal of Cobalt (II) ions from aqueous solutions and nuclear industry wastewater using sulfhydryl and carboxyl functionalised magnetite nanocellulose composite: batch adsorption studies. Chem Ecol 2019;35(3):235–55. https://doi.org/10.1080/02757540.2018.1532999.

[11] Narwade VN, Khairnar RS, Kokol V. In situ synthesized hydroxyapatite—cellulose nanofibrils as biosorbents for heavy metal ions removal. J Polym Environ 2018;26:2130–41. https://doi.org/10.1007/s10924-017-1101-7.

[12] Segal L, Creely JJ, Martin AE, Conrad CM. An empirical method for estimating the degree of crystallinity of native cellulose using the X-ray diffractometer. Textil Res J 1959;29(10):786–94. https://doi.org/10.1177/004051755902901003.

[13] Wulandari WT, Rochliadi A, Arcana IM. Nanocellulose prepared by acid hydrolysis of isolated cellulose from sugarcane bagasse. IOP Conf Ser Mater Sci Eng 2016;107(1):1–7. https://doi.org/10.1088/1757-899X/107/1/012045.

[14] Jin E, Guo J, Yang F, Zhu Y, Song J, Jin Y, et al. On the polymorphic and morphological changes of cellulose nanocrystals (CNC-I) upon mercerization and conversion to CNC-II. Carbohydr Polym 2016;143:327–35. https://doi.org/10.1016/j.carbpol.2016.01.048.

[15] Isogai A, Saito T, Fukuzumi H. TEMPO-oxidized cellulose nanofibers. Nanoscale 2011;3:71–85. https://doi.org/10.1039/C0NR00583E.

[16] Saito T, Kimura S, Nishiyama Y, Isogai A. Cellulose nanofibers prepared by TEMPO-mediated oxidation of native cellulose. Biomacromolecules 2007;8:2485–91. https://doi.org/10.1021/bm0703970.

[17] Sirviö JA, Kolehmainen A, Visanko M, Liimatainen H, Niinimäki J, Hormi OEO. Strong, self-standing oxygen barrier films from nanocelluloses modified with regioselective oxidative treatments. ACS Appl Mater Interfaces 2014;6(16):14384–90. https://doi.org/10.1021/am503659j.
[18] Zhang K, Shen M, Liu H, Shang S, Wang D, Liimatainen H. Facile synthesis of palladium and gold nanoparticles by using dialdehyde nanocellulose as template and reducing agent. Carbohydr Polym 2018;186:132–9. https://doi.org/10.1016/j.carbpol.2018.01.048.
[19] Mathias SL, Menezes AJ, Longaresi RH, Da Silva MP. Caracterização e obtenção de Nanocristais De Celulose De Diferentes Estádios Fenológicos Da Planta De Milho (Zea Mays L.). In: Anais do 14º Congresso Brasileiro de Polímeros. 14; 2017. p. 1132–6.
[20] Morán JI, Alvarez VA, Cyras VP, Vázquez A. Extraction of cellulose and preparation of nanocellulose from sisal fibers. Cellulose 2008;15(1):149–59. https://doi.org/10.1007/s10570-007-9145-9.
[21] Kvien I, Tanem BS, Oksman K. Characterization of cellulose whiskers and their nanocomposites by atomic force and electron microscopy. Biomacromolecules 2005;6(6):3160–5. https://doi.org/10.1021/bm050479t.
[22] Reid MS, Villalobos M, Cranston ED. Benchmarking cellulose nanocrystals: from the laboratory to industrial production. Langmuir 2017;33(7):1583–98. https://doi.org/10.1021/acs.langmuir.6b03765.
[23] George J, Sabapathi SN. Cellulose nanocrystals: synthesis, functional properties, and applications. Nanotechnol Sci Appl 2015;8:45–54. https://doi.org/10.2147/NSA.S64386.
[24] Chattopadhyay D, Patel BH. Synthesis, characterization and application of nano cellulose for enhanced performance of textiles. J Textile Sci Eng Res Arti 2016. https://doi.org/10.4172/2165-8064.1000248.
[25] Jiang F, Hsieh YL. Chemically and mechanically isolated nanocellulose and their self-assembled structures. Carbohydr Polym 2013;95:32–40. https://doi.org/10.1016/j.carbpol.2013.02.022.
[26] Gu J, Catchmark JM, Kaiser EQ, Archibald DD. Quantification of cellulose nanowhiskers sulfate esterification levels. Carbohydr Polym 2013;92:1809–16. https://doi.org/10.1016/j.carbpol.2012.10.078.
[27] Nishiyama Y, Sugiyama J, Chanzy H, Langan P. Crystal structure and hydrogen bonding system in cellulose Iα from synchrotron X-ray and neutron fiber diffraction. J Am Chem Soc 2003;125(47):14300–6. https://doi.org/10.1021/ja0257319.
[28] Hai LV, Zhai L, Kim HC, Kim JW, Choi ES, Kim J. Cellulose nanofibers isolated by TEMPO-oxidation and aqueous counter collision methods. Carbohydr Polym 2018;191:65–70. https://doi.org/10.1016/j.carbpol.2018.03.008.
[29] Teixeira EM, Corrêa AC, Manzoli A, Leite FL, Oliveira CR, Mattoso LHC. Cellulose nanofibers from white and naturally colored cotton fibers. Cellulose 2010;17:595–606. https://doi.org/10.1007/s10570-010-9403-0.
[30] Teodoro KBR, Teixeira EM, Corrêa AC, Campos A, Marconcini JM, Mattoso LHC. Whiskers de fibra de sisal obtidos sob diferentes condições de hidrólise ácida: efeito do tempo e da temperatura de extração. Polymers 2011;21:280–5. https://doi.org/10.1590/S0104-14282011005000048.
[31] Roine A. HSC-chemistry for windows. Pori, Finland: Outokumpu Research Oy; 2006.
[32] Druval S, Bustamante RA, Rocha CER, Silva VD, Rodrigues EJR, Müller CDB, et al. Fabrication of lignocellulose-based microreactors: copper functionalized Bamboo for continuous-flow CuAAC click reactions. Sustain Chem. Eng. 2019;7(3):3267–73. https://doi.org/10.1021/acssuschemeng.8b05273.